Paramagnetic Resonance Absorption of Mn^{++} in Single Crystals of $CaCO_3$*†

F. KENNETH HURD,‡ MENDEL SACHS, AND W. D. HERSHBERGER
University of California, Los Angeles, California
(Received August 17, 1953)

Paramagnetic resonance absorption of Mn^{++} at 9300 Mc/sec has been studied using single crystals of $CaCO_3$ containing 0.06 wt. percent Mn^{++} ions. The Mn^{++} spectrum consists of 30 well-resolved lines approximately 3.5 gauss wide and extending over a range of 1100 gauss with a large dependence upon angular orientation between crystal axes and external magnetic field. The theory pertaining to the Mn^{++} resonance absorption in the $CaCO_3$ crystal is developed and presented. The interpretation of the observed spectra is based upon crystalline field effects plus nuclear hyperfine interaction. The spectroscopic g factor is found to be essentially isotropic. The hyperfine structure factors A' and B' are found to be nearly equal. The fine structure constants D' and d' are determined. The values assigned are:

$$g_{\parallel}=2.0022, \quad g_{\perp}=2.0014, \quad A'=8.782\times10^{-3}\ \text{cm}^{-1},$$
$$D'=3.75\times10^{-3}\ \text{cm}^{-1}, \quad d'=4.00\times10^{-6}\ \text{cm}^{-1}, \quad B'=8.774\times10^{-3}\ \text{cm}^{-1}.$$

Small discrepancies between theory and experiment are found, as well as unexpected and unexplained line-splittings at certain angular orientations.

INTRODUCTION

INVESTIGATION of the effects of crystalline fields on paramagnetic resonance absorption spectra contributes to our knowledge of the solid state by revealing certain properties of the crystal and of the paramagnetic ion. They theory describing paramagnetic resonance in crystals is necessarily based upon a single crystal model. Several investigators[1] have observed and interpreted spectra in single crystals of alums, Tutton salts, and similar materials in which the crystalline field is that of the surrounding waters of hydration. Single crystals of non-hydrated inorganic compounds with suitable substitutional concentration of the paramagnetic ions have been unobtainable, and hence studies of these materials have previously been limited to powdered samples[2,3] which presumably consist of a large number of randomly oriented crystals. In the resulting spectrum, angular dependent effects are average; thus information about anisotropic crystalline fields is obscured. The present investigation used single $CaCO_3$ crystals of the calcite structure with 0.06 wt. percent Mn as a substitutional impurity. The calcite structure has trigonal symmetry in the nearest neighbors (the CO_3^{--} ions) and cubic symmetry in the next nearest neighbors (Ca^{++}). The 9300-Mc/sec paramagnetic resonance absorption spectra of the Mn^{++} observed in these crystals exhibited a large anisotropy as was to be expected for the trigonal field. Since the lines have a width of only 3.5 gauss, and their positions were determined with an accuracy of one gauss using proton resonance and since the effect of angular orientation on line position is large, the present work with calcite permits a precise comparison between the predictions of theory and experimental observations themselves. On the whole, the agreement between theoretical predictions and the results of experiment is good; however, small deviations greater than the experimental error are found, as well as a heretofore unobserved splitting of certain lines which depends upon angle.

THEORY

The predominant features of the magnetic behavior of doubly ionized manganese occurring substitutionally in a single crystal of calcium carbonate should be explained in terms of the D_3 point group symmetry[4] of the neighboring carbonate radicals and the magnetic interaction between the electronic and nuclear moments of the manganese ion.

FINE STRUCTURE

The fine structure splitting is caused by the crystalline field which leaves the magnetic levels doubly degenerate and the external magnetic field which lifts this degeneracy. The ground state of Mn^{++} is a ${}^6S_{\frac{5}{2}}$ state, and the nuclear spin is $I=5/2$. The total number of energy levels is $(2S+1)(2I+1)=36$. The selection rules for paramagnetic resonance absorption are $\Delta M=+1$, $\Delta m=0$ (where M and m are the electronic and nuclear magnetic quantum numbers respectively); hence the total number of transitions is 30.

The most general expression for the crystalline potential at the site of the Manganese nucleus is given by

$$V=\sum_{l=0}^{\infty}\sum_{m=-l}^{+l}\Lambda_l{}^m r^l Y_{lm}(\theta,\varphi), \tag{1}$$

where $\Lambda_l{}^m$ is the crystal field coefficient, r is the radius

* A preliminary account of this work was given by M. Sachs, Bull. Am. Phys. Soc. **28**, No. 6, 15 (1953).

† Work supported in part by the U. S. Office of Naval Research.

‡ Present address: Visiting Fulbright Professor, Fouad University, Cairo, Egypt.

[1] See W. Gordy *et al.*, *Microwave Spectroscopy* (John Wiley and Sons, Inc., New York, 1953) for a comprehensive bibliography to July, 1952.

[2] E. E. Schneider and T. S. England, Physica **17**, 221 (1951).

[3] W. D. Hershberger and H. N. Leifer, Phys. Rev. **88**, 714 (1952).

[4] Eyring, Walter and Kimball, *Quantum Chemistry* (John Wiley and Sons, Inc., New York, 1947).

of the magnetic ion, and $Y_{lm}(\theta,\varphi)$ is a spherical harmonic $P_l^m(\cos\theta)e^{im\varphi}$.

The calculation of the expectation value of the crystalline potential requires integration between d wave functions. The product $\psi_{3d}^*\psi_{3d}$ transforms under rotation like the base vector of the direct product $D_2\times D_2$ of the representations of the rotation group. Since the direct product

$$D_2\times D_2=\sum_{L=0}^{4} D_L,$$

the components of the potential V with $l>4$ will have vanishing diagonal matrix elements. The odd l components of the potential V are off diagonal in the orbital quantum number l. Since the excited orbitals are very far from the ground state, these components of V can be neglected.

Assuming the crystalline potential to be axial, the fine structure Hamiltonian $\mathfrak{IC}_{fs}$ is

$$\begin{aligned}\mathfrak{IC}_{fs}&=\mathfrak{y}\cdot\mathbf{H}+V\\&=H(\mu_{x'}\sin\theta'\cos\varphi'+\mu_{y'}\sin\theta'\sin\varphi'+\mu_{z'}\cos\theta')\\&\quad+\Lambda_2^0\gamma^2P_2(\cos\theta')+\Lambda_4^0\gamma^4P_4(\cos\theta'),\end{aligned}\quad(2)$$

where $(x',\ y',\ z')$ refer to the crystalline coordinate system and P_l is the Legendre polynomial.

In the case under study, the magnetic energy is much larger than the crystalline energy; hence the Hamiltonian (2) must be quantized with respect to the direction of magnetization in the crystal (z axis).

In order to rotate the Hamiltonian (2) from the primed to the unprimed frame of reference, use is made of the spherical harmonic addition theorem.

$$P_l(\cos\theta')=\frac{4\pi}{2l+1}\sum_{m=-l}^{+l}\bar{P}_l^m(\cos\bar{\theta})\bar{P}_l^m(\cos\theta'')e^{im(\bar{\varphi}-\varphi'')},\quad(3)$$

where $\bar{P}_l^m$ is the normalized associated Legendre polynomial, $\bar{\theta}$ is the angle between the radial vector and the direction of magnetization, and θ'' is the angle between the direction of magnetization and the crystalline field axis.

The rotated Hamiltonian (2) is

$$\begin{aligned}\mathfrak{IC}_{fs}&=\mu_zH_z+(4\pi/5)\Lambda_2^0\gamma^2\sum_{m=-2}^{+2}\bar{P}_2^m(\cos\bar{\theta})\\&\quad\times\bar{P}_2^m(\cos\theta'')e^{im(\bar{\varphi}-\varphi'')}+(4\pi/9)\Lambda_4^0\gamma^4\\&\quad\times\sum_{m=-4}^{+4}\bar{P}_4^m(\cos\bar{\theta})\bar{P}_4^m(\cos\theta'')e^{im(\bar{\varphi}-\varphi'')}.\end{aligned}\quad(4)$$

The eigenvalues of the Hamiltonian (4) will be calculated by first and second order perturbation theory. The matrix elements of the crystalline terms are diagonal when $m=0$, the matrix elements of the remaining terms in the summation are off diagonal, and their eigenvalues must be calculated by second-order perturbation theory. The second-order terms for the third factor in Eq. (4) will be neglected because of the small order of magnitude of Λ_4^0. The matrix elements of $P_l^m(\cos\bar{\theta})$ are evaluated by noting that since they transform under rotation like the base vector of the D_l representation of the rotation group, their matrix elements have the same dependence on the magnetic quantum number M as the Wigner coefficients $S_{JMM_L}^{(LS)}$.[5] Hence, the matrix element of the associated Legendre polynomial is the product of the Wigner coefficient and a factor which depends upon the total angular quantum numbers of the ion but which is independent of M. Since the amount of orbital momentum produced by the crystalline-field distortion of the S state is unknown, these constants cannot be evaluated but will be left as empirical constants γ and δ. In the cases where the total quantum numbers are known (i.e., paramagnetic salts of the rare earth ions), these constants can be evaluated by the method described by Stevens.[6]

The matrix elements of the Legendre polynomials are

$$\begin{aligned}(M\,|\,P_2^0\,|\,M)&=\gamma[3M^2-S(S+1)],\\(M\,|\,P_2^1\,|\,M\pm1)&=\gamma\{(1\pm2M)[(3/2)(S\pm M+1)\\&\quad\times(S\mp M)]^{\frac{1}{2}}\},\\(M\,|\,P_2^2\,|\,M\pm2)&=\gamma[(3/2)(S\pm M+2)(S\pm M+1)\\&\quad\times(S\mp M)(S\mp M-1)]^{\frac{1}{2}},\\(M\,|\,P_4^0\,|\,M)&=\delta[35M^4-30S(S+1)M^2+25M^2\\&\quad-6S(S+1)+3S^2(S+1)^2].\end{aligned}\quad(5)$$

Making use of Eq. (5), the eigenvalues of the Hamiltonian (4) become

$$\begin{aligned}E_M^{fs}&=g\beta HM+D'[(M^2-(1/3)S(S+1)]\\&\quad\times[(3g_{\|}^2/g^2)\cos^2\theta-1]\\&\quad-\frac{2D'^2}{g\beta H_0}[M(4S(S+1)-1)-8M^3]\\&\quad\times\frac{g_{\|}^2g_{\perp}^2}{g^4}\sin^2\theta\cos^2\theta\\&\quad+\frac{D'^2}{2g\beta H_0}[M(2S(S+1)-1)+2M^3]\\&\quad\times(g_{\perp}^4/g^4)\sin^4\theta+d'[35M^4-30S(S+1)M^2\\&\quad+25M^2-6S(S+1)+3S^2(S+1)^2]\\&\quad\cdot\left(35\frac{g_{\|}^4}{g^4}\cos^4\theta-30\frac{g_{\|}^2}{g^2}\cos^2\theta+3\right),\end{aligned}\quad(6)$$

where

$$D'=(3/2)\gamma\Lambda_2^0\langle r_{3d}^2\rangle_{Av},\quad d'=(1/8)\delta\Lambda_4^0\langle r_{3d}^4\rangle_{Av},$$
$$g=[g_{\|}^2\cos^2\theta+g_{\perp}^2\sin^2\theta]^{\frac{1}{2}},\quad\cos\theta''=(g_{\|}/g)\cos\theta$$

[5] E. Wigner, *Gruppentheorie* (Edwards Brothers, Inc., Ann Arbor, 1931).

[6] K. W. H. Stevens, Proc. Phys. Soc. (London) **A65**, 209 (1952).

and where θ is the angle between the magnetic field H and the crystalline field axis, and $g_{\parallel}$ and $g_{\perp}$ are the components of the spectroscopic splitting factor parallel and perpendicular to the crystalline-field axis, respectively. The d' term neglected by Bleaney[7] is of sufficient magnitude to be required in the interpretation of spectra exhibiting large axial crystalline-field effects.

HYPERFINE STRUCTURE

The hyperfine splitting is the result of a coupling between nuclear and electronic magnetic moments. The hyperfine structure Hamiltonian ($\mathcal{H}_{\rm hfs}$) is

$$\mathcal{H}_{\rm hfs}=AS_zI_z+\tfrac{1}{2}B(S_+I_-+S_-I_+), \tag{7}$$

where $S_\pm=S_x\pm iS_y$ and $I_\pm=I_x\pm iI_y$. S is the effective electronic spin, and I is the nuclear spin.

The eigenvalues of $\mathcal{H}_{\rm hfs}$ are angularly dependent if A is not equal to B.[7] In the case under study, A is approximately equal to B; consequently the angular dependence of higher-order perturbation terms will be neglected. The eigenvalues of (7) calculated by first-, second-, and fourth-order perturbation theory are

$$\begin{aligned}E_{Mm}{}^{\rm hfs}=K'Mm&+\frac{A'^2}{2g\beta H_0}\{M[I(I+1)-m^2]\\&-m[(S(S+1)-M^2]\}\\&+\frac{A'^4}{(2g\beta H_0)^3}[m^3\sigma(S)-M^3\sigma(I)+M^2m^3\tau(S)\\&-M^3m^2\tau(I)+M^4m\xi(I)-Mm^4\xi(S)\\&+m\eta_S(I)-M\eta_I(S)+Mm^2\zeta_S(I)\\&-M^2m\zeta_I(S)+M^3m^4-M^4m^3],\end{aligned} \tag{8}$$

where

$$\begin{aligned}&\sigma(x)=x(x+1)[4-3x(x+1)],\\&\tau(x)=[6x(x+1)-9],\quad \xi(x)=[3x(x+1)-1],\\&\eta_x(y)=[3x^2(x+1)^2y(y+1)-x^2(x+1)^2\\&\qquad-4x(x+1)y(y+1)+2x(x+1)],\\&\zeta_x(y)=[6x(x+1)y(y+1)-11x(x+1)-2y(y+1)+5],\\&K'=(1/g)[A'^2g_{\parallel}{}^2\cos^2\theta+B'^2g_{\perp}{}^2\sin^2\theta]^{\frac{1}{2}}.\end{aligned}$$

Combining Eqs. (6) and (8), we obtain the total energy eigenvalue:

$$E_{Mm}=E_M{}^{\rm fs}+E_{Mm}{}^{\rm hfs}, \tag{9a}$$

and the transition energy:

$$h\nu_0=E_{Mm}-E_{M-1,m}. \tag{9b}$$

Since in paramagnetic resonance absorption experiments the radiation frequency is kept constant and the magnetic field is varied, Eq. 9(b) is solved for H and the line position becomes (in units of gauss):

$$\begin{aligned}H=H_0&-D(2M-1)\left(3\frac{g_{\parallel}{}^2}{g^2}\cos^2\theta-1\right)\\&+\frac{2D^2}{H_0}[4S(S+1)-24M(M-1)-9]\\&\times\frac{g_{\parallel}{}^2g_{\perp}{}^2}{g^4}\sin^2\theta\cos^2\theta\\&-\frac{D^2}{2H_0}[2S(S+1)-6M(M-1)-3]\frac{g_{\perp}{}^2}{g^4}\sin^4\theta\\&-d\{140M^3-210M^2+[190-60S(S+1)]M\\&+30S(S+1)-60\}(35(g_{\parallel}{}^4/g^4)\cos^4\theta\\&-30(g_{\parallel}{}^2/g^2)\cos^2\theta+3)-Km\\&-\frac{A^2}{2H_0}[I(I+1)-m^2+m(2M-1)]\\&-\frac{A^4}{8H_0{}^3}\{(4M^3-6M^2+4M-1)[m\xi(I)-m^3]\\&+(3M^2-3M+1)[m^4-m^2\tau(I)-\sigma(I)]\\&+(2M-1)[m^3\tau(S)-m\zeta_I(S)]\\&+m^2\zeta_S(I)-m^4\xi(S)-\eta_I(S)\},\end{aligned} \tag{10}$$

where $D=D'/g\beta$, $d=d'/g\beta$, $H_0=h\nu_0/g\beta$, $A=A'/g\beta$, and $B=B'/g\beta$.

INTENSITIES

The observed transitions may be identified with electronic quantum numbers by means of their intensities. The intensity of magnetic dipole radiation is proportional to $(J+M)(J-M+1)$. Hence the intensities of transitions between the Zeeman levels of Mn^{++} occur in the ratios (the subscript denotes the upper of the two magnetic levels):

$$I_{\frac{5}{2}}:I_{\frac{3}{2}}:I_{\frac{1}{2}}:I_{-\frac{1}{2}}:I_{-\frac{3}{2}}=5:8:9:8:5. \tag{11}$$

EXPERIMENTAL METHOD

The crystals were prepared by cleaving them along the natural rhomdehedral cleavage planes of calcite to a size approximately 4 mm on a side and mounted at the desired orientation with wax onto a $\frac{1}{8}$-in. quartz rod. The orientation of the crystal with respect to the quartz rod was checked by means of optical gainiometer measurements and held to a precision of 20 min of arc.

Two mountings were used, one such that the c-crystallographic axis (which incidentally is the optic axis) was parallel to the axis of the quartz rod and a second with the c axis perpendicular to the axis of the quartz rod. Inasmuch as the crystalline electric field in calcite is

[7] B. Bleaney, Phil. Mag. 42, 441 (1951).

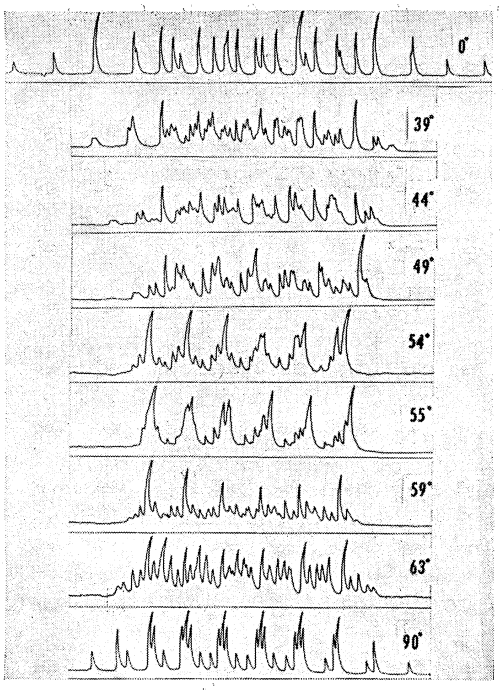

FIG. 1. Direct 9300-Mc/sec absorption curves of Mn^{++} 0.06 wt. percent in a single crystal of $CaCO_3$. The angle specified is that between the c-crystallographic axis and the external magnetic field. The 0° curve extends from 2732 gauss to 3872 gauss. The individual lines are symmetrical. The apparent asymmetry is due to the curvilinear coordinate of the Brush recorder.

predominately axial and lies along the c axis, most of the data were obtained with the latter crystal.

The experimental method was the same as that used by Hershberger and Leifer[3] in their investigation of powdered phosphors except for the method of mounting the sample and the method of measurement of the magnetic field. The crystals used in this investigation were natural calcite crystals which by chemical analysis were found to contain 6.02×10^{-3} wt. percent of Mn. The crystals cleaved along natural cleavage planes were mounted on a quartz rod which in turn was mounted in a holder which formed the end wall of a cylindrical resonant cavity operated in the circular electric or TE_{011} mode. The holder placed the quartz rod along the axis of the cavity and the sample at the center of the cavity. The holder was rotatable and graduated so that the crystal could be rotated through known angles. The resonant cavity placed in the magnetic field with its axis perpendicular to the externally applied magnetic field satisfied the condition for resonance, that is, rf magnetic field perpendicular to external magnetic field.

The general features of the detection systems have been previously described[3] and will be reviewed briefly to point out some modification with regard to field measurement.

The magnetic field is swept over the 1200-gauss range in approximately 10 min and is simultaneously swept 1 or 2 gauss at a 35-cps rate. The low-speed wide-range sweep is accomplished by varying the set point on an electronic regulator supply furnishing power for the main magnet coils while separate low inductance coils are employed to inject the 35 cps sweep. The band width of the detection system is approximately 3 cps. Changes in power transmitted through the cavity containing the sample are amplified by a narrow band 35-cps amplifier and are then detected and recorded using a square law detector and a phase detector followed by a two-channel brush recorder. This method of detection yields the derivative of the absorption curve but with a loss of its sign for the square law detector. Signals-to-noise ratios in excess of 1000 were obtained for samples of approximately $\frac{1}{8}$ gram and 6×10^{-2} wt. percent Mn, indicating that less than 10^{15} Mn^{++} ions may be detected.

The large signal-to-noise ratio permitted dc amplification of the transmitted power changes, yielding the absorption curves directly. Some such curves are shown in Fig. 1.

Magnetic field strength is measured by means of proton resonance. The proton resonance signal is detected and used as the information signal of a servo system which adjusts the proton resonance oscillator, keeping it centered on the proper frequency for the magnetic field. Hence, as the magnetic field is driven slowly through the desired range, the proton resonance oscillator follows automatically. The oscillator is hetrodyned with the harmonics of a General Radio Type 1100-A Secondary frequency standard, which are spaced at 100-kc/sec intervals. The hetrodyne signal is detected and amplified by a narrow-band low-frequency amplifier, such that zero beat gives an impulse to the marker pen on the brush recorder. These markers appear every 100 kc/sec which corresponds to approximately 23.5 gauss. The markers can be seen in Fig. 2. Actual data were taken from records for which the paper speed was greater than that shown in the figure in order to reduce the interpolation error. Linear interpolation is used between markers. The stability of the magnetic field and the tracking of the servo system are such that the maximum uncertainty of a field determination is approximately 1 gauss.

EXPERIMENTAL RESULTS

It was anticipated that the axial component of the crystalline electric field would be parallel the c axis of the crystal. To test the correctness of this assumption, one crystal was mounted with the c axis parallel ($c\parallel$) to the quartz rod, and data were taken every 10° for a total rotation of the crystal of 180°. Thus the c axis was kept perpendicular to the external magnetic field for all angular orientations. No angular change in the line position was noted; hence it was concluded that the (large) axial crystalline-electric field had no component perpendicular to the c axis and in fact coincided with the c axis.

A second crystal was mounted with the c axis per-

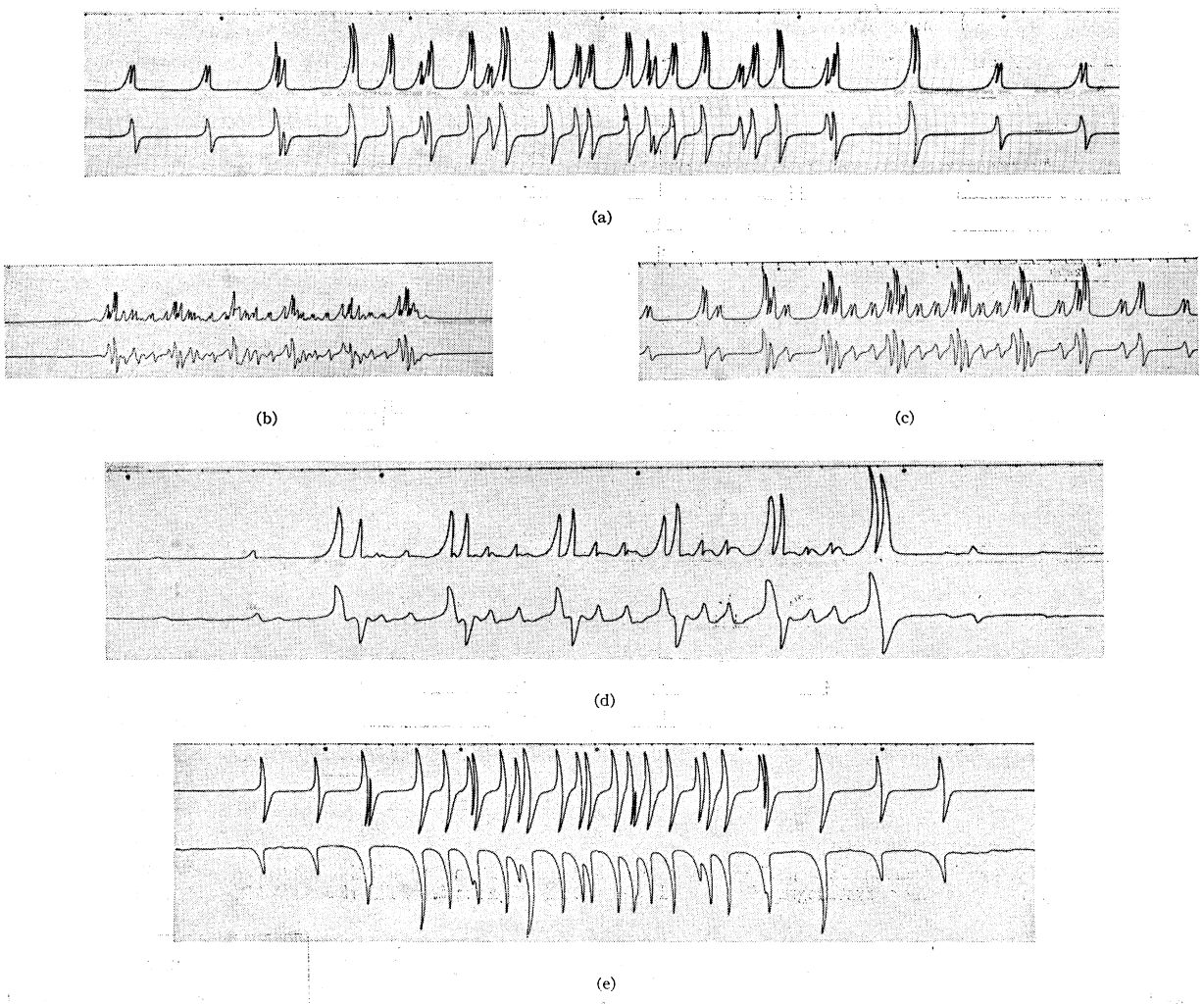

FIG. 2. Experimental records for $CaCO_3$:Mn 0.06 wt. percent. (a) $\theta=0°$; (b) $\theta=57°$; (c) $\theta=90°$; (d) powdered; (e) $\theta=0°$. Rf=9300 Mc/sec. The slope of the absorption curve is recorded except in the lower $\theta=0°$ case where the relationship between the slope and direct absorption is shown. The magnetic field markers appear at the top of the records.

pendicular ($c\perp$) to the quartz rod. Rotation for this crystal permitted orientation of the axial crystalline field with respect to the external magnetic field to any desired angle between 0° and 360°. Inasmuch as the mount did not allow absolute correlation between the c axis and the angular scale, the correlation was obtained experimentally at 90° by comparison between the $c\parallel$ and $c\perp$ data. A precision of 1° in the angular determination was obtained.

The angular dependence of the line positions is shown in Fig. 1 which record absorption directly. Figure 3 plots the $m=+5/2$ and $m=-5/2$ lines for the angles at which they may be determined with precision. It will be noted from Fig. 1 that many of the lines can be neither clearly resolved nor positively identified for angles between 0° and 90°. Note both in Figs. 1 and 3 the splitting of the $M=+5/2$, $+3/2$, $-1/2$, and $-3/2$ lines at intermediate orientations between 0°, 90°, and 180°. Figure 4 shows the angular dependence of the central ($M=+1/2$) lines to an enlarged scale where deviations from the line position at 90° are plotted for each of the six central ($M=+1/2$) lines. It is noted that the magnitude of the angular dependence is a function of the nuclear magnetic quantum number m increasing monotonically from $m=+5/2$ to $m=-5/2$, although the increase does not seem to be linear. The evidence of nonlinearity is not conclusive since overlapping of the lines reduces the precision at the angles where the shift is the greatest.

Figure 2 shows the appearance of the spectrum at 0°, 57°, 90°, and for a sample of the calcite which was powdered by grinding to give random crystal orientation. At 0° and at 90°, most of the 30 lines are seen to be well resolved. For this reason and for the reason that the theoretical expression for the line positions have maxima or minima in the angular dependent terms at these angles, they were chosen for precision measurements, and the interpretation is based principally upon

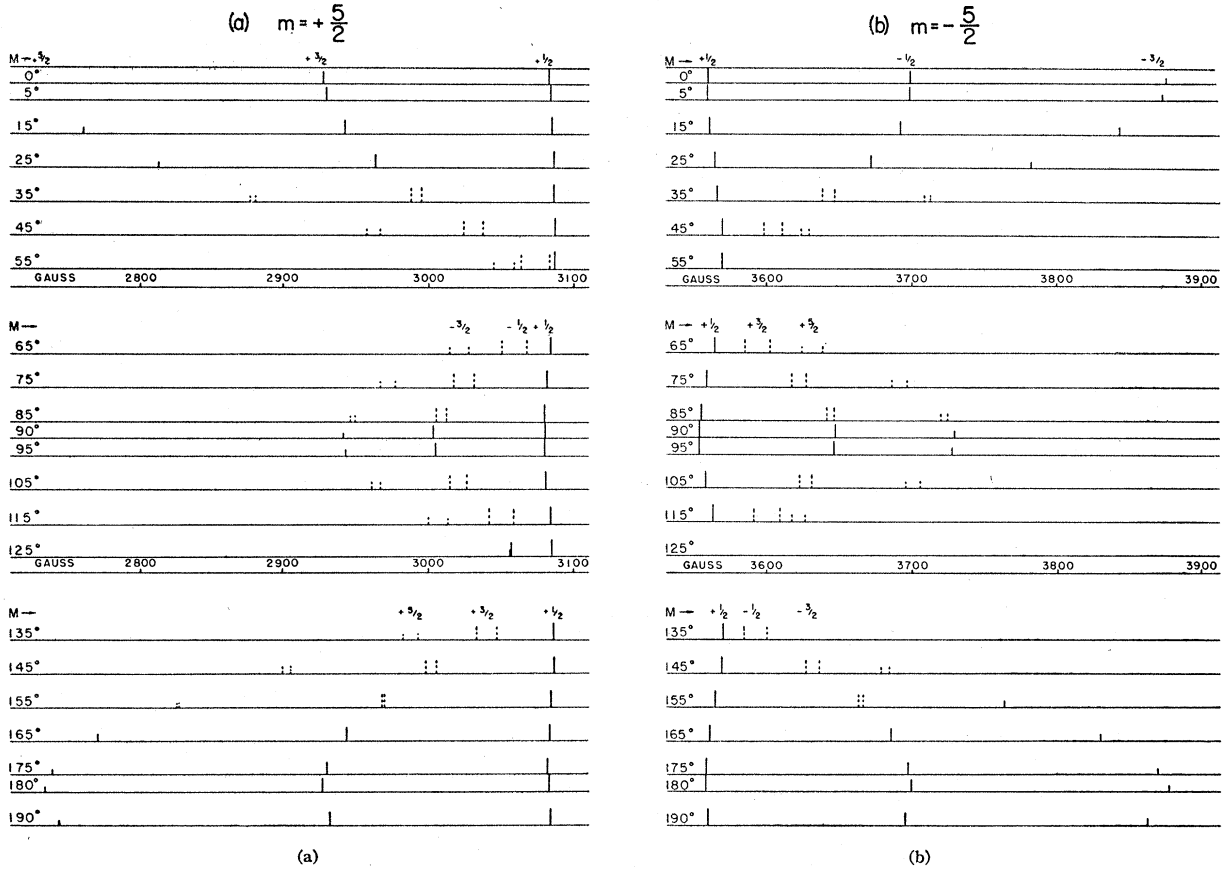

FIG. 3. Mn^{++} 0.06 wt. percent in $CaCO_3$. The angular dependent line position and splitting for the $m=\pm 5/2$ lines are shown for certain angles between the c-crystallographic axis and the external magnetic field. The rf is 9300 Mc/sec. (a) $m=+5/2$; (b) $m=-5/2$.

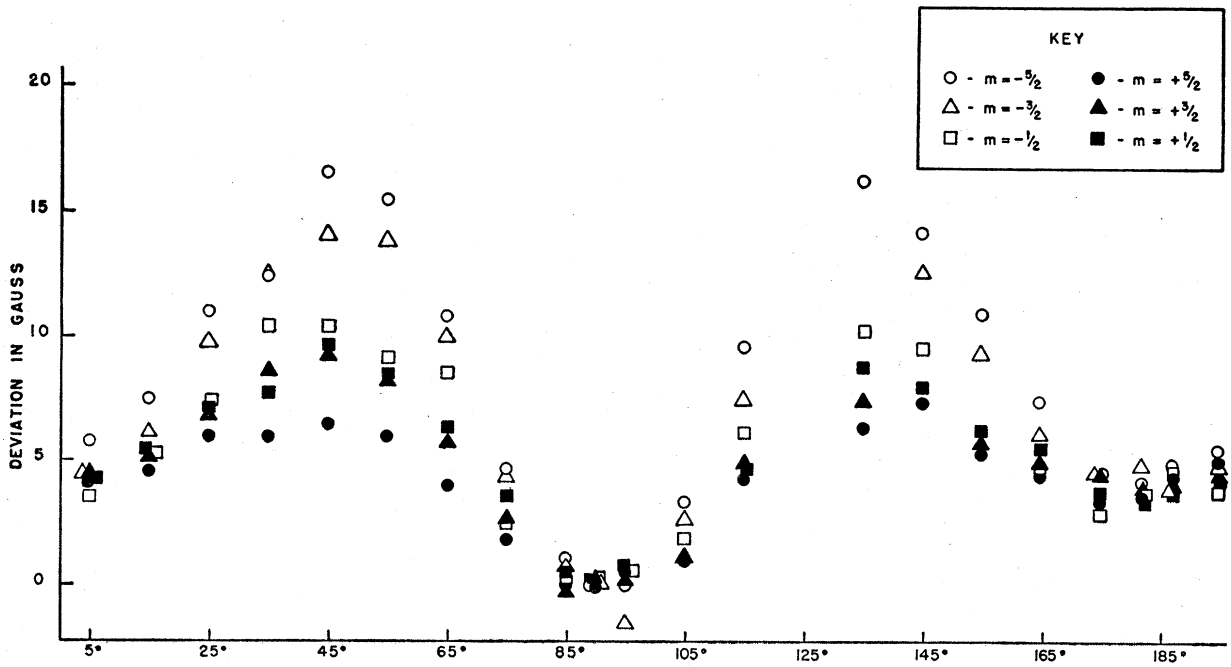

FIG. 4. Mn^{++} 0.06 wt. percent in $CaCO_3$; rf=9300 Mc/sec. The angular dependence of the $M=+1/2$ lines is shown in terms of deviation from their position at $\theta=90°$. The angle θ is the angle between the c-crystallographic axis and the external magnetic field.

line positions at these two angles. The "powdered" curve shows angular dependence of the central $M=+1/2$ lines as a function of m. The $m=+5/2$ line is the strong line on the right (low field) and the $m=-5/2$ line is on the left. Increased angular dependence from $m=+5/2$ to $m=-5/2$ for these randomly oriented crystals shows up as a decreased maximum slope and as an increased separation between maximum slope points. A direct absorption curve for the powdered sample is shown in Fig. 5. Figure 5 also shows a direct absorption curve to a compressed horizontal scale. The major features shown are six major ($M=+1/2$) peaks plus

TABLE I. Resonance absorption lines (in gauss) for $CaCO_3$:Mn 0.06 wt. percent, rf=9300 Mc/sec. Line positions are known to ±1.0 gauss.

M	m	$\theta=0°$	$\theta=90°$
5/2	+5/2	2732.6	3226.2
	+3/2	2826.8	3319.9
	+1/2	2924.2	3415.8
	−1/2	3022.7	3515.0
	−3/2	3125.4	3617.9
	−5/2	3232.0[a]	3725.0
3/2	+5/2	2924.2	3157.9
	+3/2	3015.9	3248.8
	+1/2	3109.8	3342.1
	−1/2	3206.9	3439.1
	−3/2	3306.1	3538.6
	−5/2	3410.0[a]	3640.9
1/2	+5/2	3080.5	3077.4
	+3/2	3169.9	3166.5
	+1/2	3260.9	3258.1
	−1/2	3354.8	3352.2
	−3/2	3451.3	3447.9
	−5/2	3550.6	3546.7
−1/2	+5/2	3236.1	3000.4
	+3/2	3322.3	3087.7
	+1/2	3410.0[a]	3176.8
	−1/2	3503.0	3268.8
	−3/2	3596.9	3362.1
	−5/2	3693.3	3457.9
−3/2	+5/2	3428.1	2938.2
	+3/2	3510.9	3023.7
	+1/2	3596.9	3111.9
	−1/2	3687.1	3201.1
	−3/2	3778.4	3292.2
	−5/2	3872.4	3385.0

[a] Because of superpositions of lines, the accuracy here is ±2.5 gauss.

secondary peaks superposed upon a broad absorption curve. The powdered crystal curves also show the futility of an attempt to interpret data regarding crystalline fields when obtained from powdered samples.

The line position for each of the 30 lines at 0° and at 90° is tabulated in Table I. Figure 6 shows a plot of the line positions at 0° and 90° with the quantum number assignments indicated.

INTERPRETATION

In accordance with the customary practice, the lines are designated by the quantum numbers of the upper energy level involved in the transition corresponding to

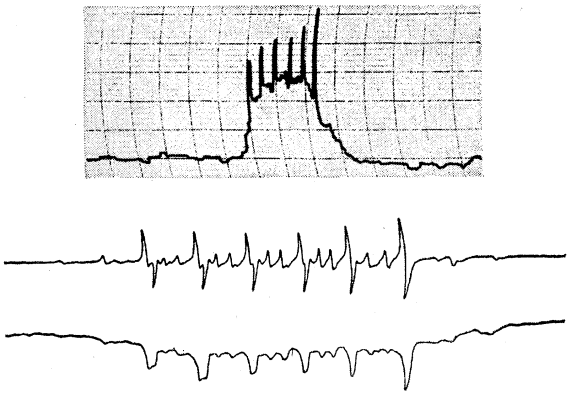

FIG. 5. Spectrum for a sample of $CaCO_3$:Mn 0.06 wt. percent, powdered by grinding. The direct absorption spectrum and its slope are shown below. The direct absorption spectrum to a compressed scale is shown above.

the line. Thus the line associated with the $M=+3/2\rightarrow+5/2$, $m=+3/2\rightarrow+3/2$ transition is designated $M=+5/2$, $m=+3/2$.

The lines intensities fall into three groups as predicted by Eq. (11). Further identification of the lines is readily accomplished by comparison with the leading fine structure and hyperfine structure terms of Eq. (10).

Empirical determination of the parameters of Eq. (10) for $\theta=0°$ yields the values $H_0=3318.6$ gauss, $D=40.5$ gauss, $d=0.0428$ gauss, $A=93.95$ gauss, and $g_\parallel=2.0022$ as given in Table II. Use of these values for the parameters gives agreement between observed and calculated line position within the estimated maximum experimental error of ±1.0 gauss.

The values of the parameters which give the best

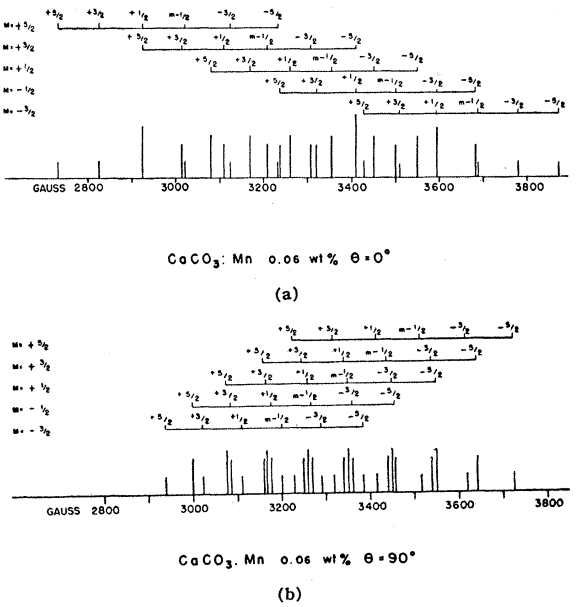

FIG. 6. Line positions and quantum number assignments. θ is the angle between the c-crystallographic axis and the external magnetic field. Rf=9300 Mc/sec.

TABLE II. Empirical values of the parameters for Mn^{++} in $CaCO_3$.[a]

	$\theta=0°$ gauss	$\theta=90°$ gauss
H_0	3318.6±1.0	3319.8±1.0
D	40.5±0.2	39.7±0.2
d	0.0428±0.002	0.0428±0.002
A	93.95±0.05	
B		93.90±0.05
	$cm^{-1}\times10^4$	$cm^{-1}\times10^4$
D'	37.9±0.2	37.1±0.2
d'	0.0400±0.0002	0.0400±0.0002
A'	87.82±0.08	
B'		87.74±0.08
$g_{\parallel}=2.0022\pm0.0006$		
$g_{\perp}=2.0014\pm0.0006$		

[a] A discrepancy in the two values of the constant D is noted. The value $D'=(37.5\pm0.4)\times10^{-4}$ cm^{-1} would give agreement between calculated and experimental line positions.

agreement between experimental and calculated values of line positions at 90° are $H_0=3319.8$ gauss, $D=39.7$ gauss, $d=0.0428$ gauss, $B=93.90$ gauss, $g_{\perp}=2.0014$. At this angle some difficulty is experienced in assigning best values to the parameters. The values assigned yield agreement between experimental and calculated line positions to within the maximum experimental error for all lines except the $M=+5/2$, $m=+5/2$ and the $M=-5/2$, $m=-5/2$ lines where the discrepancy is about four times the experimental error.

In an attempt to account for discrepancies, the effect of higher order terms of a trigonal symmetry, use of a small cubic symmetry contribution, and nuclear quadrupole effects have been examined and are found to be inadequate. The discrepancies, though small, are considered to be significant.

The angular dependent splitting of the $M=+5/2$, $+3/2$, $-1/2$, and $-3/2$ lines shown in Fig. 3 is unexpected. Crystalline imperfections of the lineage structure type would produce discrete angular dislocations of the crystal planes and might occur frequently enough throughout the crystal to yield two slightly different orientations of the crystal effectively, thereby giving rise to two equally intense lines of the angular dependent spacing observed. The hypothesis, although attractive, must be discarded inasmuch as it would demand the splittings for the $M=+5/2$ and $-3/2$ lines to be twice that for the $M=+3/2$ and $-1/2$ lines whereas the observation is that the $M=+5/2$, $-3/2$ lines are split less than the $M=+3/2$, $-1/2$ lines.

The significance of the crystalline-field-splitting terms D' and d' of Table II is shown in Eq. (6), where they are expressed as the products of three factors:

$$D'=(3/2)\gamma\Lambda_2{}^0\langle r_{3d}{}^2\rangle_{Av} \quad \text{and} \quad d'=(1/8)\delta\Lambda_4{}^0\langle r_{3d}{}^4\rangle_{Av}.$$

The coefficients $\Lambda_2{}^0$ and $\Lambda_4{}^0$ are the derivatives $(1/2!)(\partial^2V/\partial z^2)_0$ and $(1/4!)(\partial^4V/\partial z^4)_0$. The terms $\langle r_{3d}{}^2\rangle_{Av}$ and $\langle r_{3d}{}^4\rangle_{Av}$ are the mean square and mean fourth radii of the $3d$ shell of Mn^{++}. The terms γ and δ are numerical factors dependent upon the total angular quantum number of Mn^{++} in the crystal.

The mean square and mean forth radii can be calculated and will probably be known to a fair degree of accuracy. Experiments designed to determine the coefficients $\Lambda_2{}^0$ and $\Lambda_4{}^0$ will allow a determination of γ and δ and will therefore enable one to determine the quantity of orbital momentum introduced by means of the crystalline field distortion of the S state of Mn^{++}.

The assistance of J. S. Fuller, from whom the crystals were obtained, and of Professor R. J. Finkelstein is gratefully acknowledged. Special credit is due R. C. Mackey who was responsible for the electronic instrumentation. A detailed presentation of the instrumentation aspects of the work is in the process of preparation by Mr. Mackey and will be published in the future.

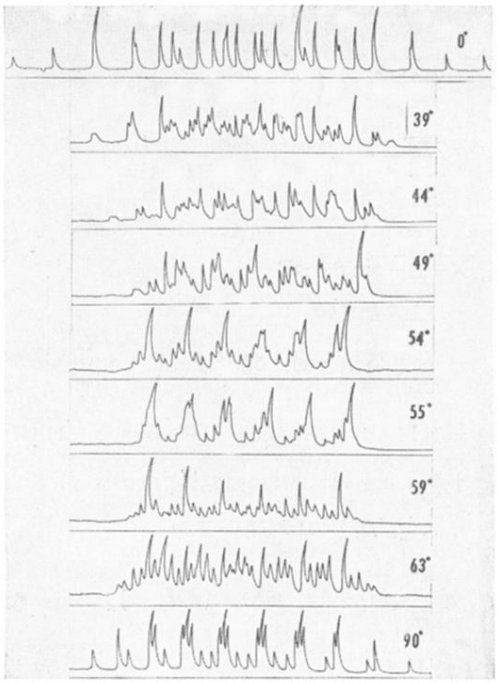

FIG. 1. Direct 9300-Mc/sec absorption curves of Mn^{++} 0.06 wt. percent in a single crystal of $CaCO_3$. The angle specified is that between the c-crystallographic axis and the external magnetic field. The 0° curve extends from 2732 gauss to 3872 gauss. The individual lines are symmetrical. The apparent asymmetry is due to the curvilinear coordinate of the Brush recorder.

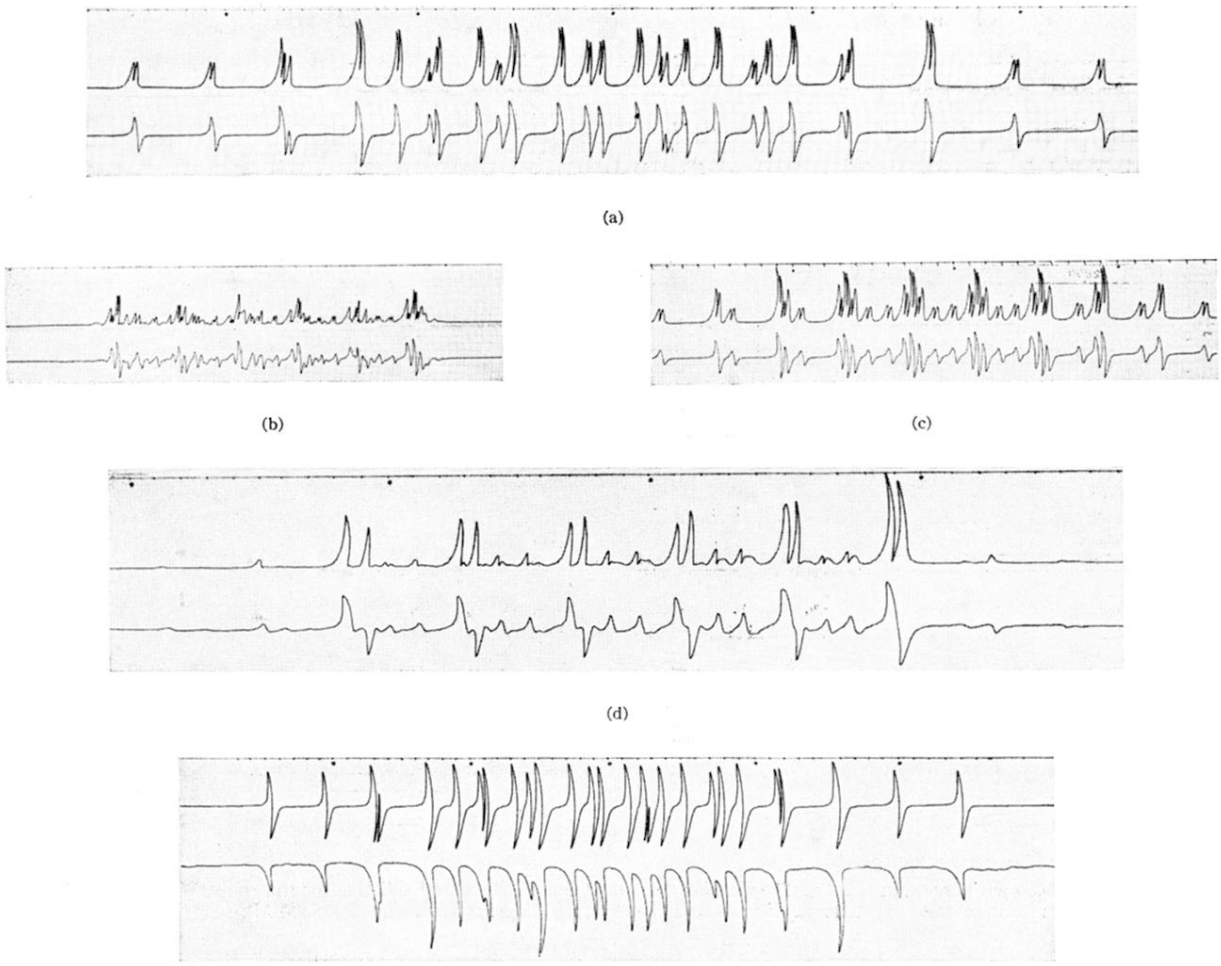

FIG. 2. Experimental records for $CaCO_3$:Mn 0.06 wt. percent. (a) $\theta=0°$; (b) $\theta=57°$; (c) $\theta=90°$; (d) powdered; (e) $\theta=0°$. Rf=9300 Mc/sec. The slope of the absorption curve is recorded except in the lower $\theta=0°$ case where the relationship between the slope and direct absorption is shown. The magnetic field markers appear at the top of the records.

FIG. 5. Spectrum for a sample of $CaCO_3$:Mn 0.06 wt. percent, powdered by grinding. The direct absorption spectrum and its slope are shown below. The direct absorption spectrum to a compressed scale is shown above.